energies

MDPI

Article

Chattering-Free Terminal Sliding Mode Control of DOC Outlet Temperature with Active Disturbance Compensation

Xiping Chen, Qinghua Jiang and Tiexiong Huang *

School of Mechanical and Marine Engineering, Beibu Gulf University, Qinzhou 535011, China; xpchen2410@163.com (X.C.); qhjiang2026@163.com (Q.J.)
* Correspondence: txhuang@bbgu.edu.cn

Abstract

Precise control of the diesel oxidation catalyst (DOC) outlet temperature is critical for reliable diesel particulate filter (DPF) regenerations. This paper proposes a novel and composite control strategy for the DOC outlet temperature control based on a representative identified transfer function model, which requires only a nominal value of the input gain parameter. By integrating a PID-type sliding variable with a non-singular terminal sliding mode (TSM) manifold through the second-order sliding mode technique, the strategy provides a continuous and chattering-free control signal. A linear extended state observer (LESO) is designed for real-time estimation and compensation of the lumped total disturbances. Feedforward compensation (FFC) is also integrated to proactively counteract the effects of exhaust flow and inlet temperature variations, thereby reducing the burden on the LESO. The disturbance rejection control scheme is designed by combining the LESO, the chattering-free terminal sliding mode (CTSM), and the FFC. Its stability is proved by using the Lyapunov method. Comprehensive co-simulations conducted in a high-fidelity GT-Power/MATLAB environment demonstrated that the proposed control scheme achieves superior performance with respect to set-point tracking and disturbance rejection. This work provides an effective solution for robust temperature control in DPF regeneration processes. It can also be applied to other types of robust process control systems attributed to its ease of implementation.

Keywords: diesel oxidation catalyst; temperature control; linear extended state observer; chattering-free terminal sliding mode; feedforward compensation

Check for updates

Academic Editor: Roberto Finesso

Received: 3 March 2026
Revised: 20 April 2026
Accepted: 28 April 2026
Published: 30 April 2026

Copyright: © 2026 by the authors. Licensee MDPI, Basel, Switzerland. This article is an open access article distributed under the terms and conditions of the Creative Commons Attribution (CC BY) license.

1. Introduction

As global regulations on diesel vehicle emissions continue to tighten, diesel particulate filter (DPF) has become an indispensable aftertreatment component for the reduction in particulate matter emissions [1–3]. During normal engine operation conditions, the DPF captures soot from the exhaust stream. However, soot accumulation increases the exhaust backpressure, degrades the engine fuel efficiency, and may even lead to filter damage. To address these issues, the accumulated soot in the filter must be periodically oxidized through a thermal regeneration process. The regeneration efficiency is highly dependent on appropriate exhaust temperatures [4,5]. However, the exhaust temperature during normal diesel vehicle operation in practice is often insufficient to sustain continuous soot oxidation [6–8], since the temperature required for DPF regeneration is ordinarily in excess of 500 °C. Therefore, a reliable thermal regeneration process relies on a diesel oxidation catalyst (DOC) and a dedicated regeneration controller [9]. To achieve the desired

exhaust temperature, diesel engines frequently employ an extra injection of fuel into the exhaust system to raise the DOC outlet temperature. The injected fuel is converted into hydrocarbons, which are then oxidized by oxygen within the DOC. This oxidation reaction releases a significant amount of heat that is required for soot combustion in the downstream filter, thereby promoting DPF regeneration [10]. However, the process of regeneration requires the consumption of additional fuel, thus necessitating a balance between the regeneration efficiency and fuel economy [11]. Imprecise temperature control can lead to either incomplete regenerations or irreversible DPF damage. Therefore, achieving precise and reliable temperature control is critical for an efficient DPF regeneration.

The DOC is a key component that provides proper heat required for DPF regeneration. However, it is a complex and nonlinear system that varies over time [12]. It is also highly susceptible to disturbances caused by the fluctuating engine operating conditions, particularly the variations in exhaust gas mass flow and temperature. Conventional control strategies struggle to address these challenges. To achieve robust disturbance rejection control, researchers have explored various advanced control approaches to the DOC outlet temperature regulation, such as model-based feedforward control [13], gain-scheduled proportional–integral–derivative (PID) control [10], internal model control (IMC) [14,15], active disturbance rejection control (ADRC) [16,17], nonlinear model predictive control [18,19], and continuous terminal sliding mode control [20]. Among these, due to its inherent robustness to system nonlinearities and uncertainties, the sliding mode control (SMC) has emerged as a particularly promising solution.

Conventional SMC ensures asymptotic stability but a finite time convergence is not guaranteed. Terminal sliding mode (TSM) control and the non-singular TSM have been developed and extended to accelerate convergence in higher-order systems by intensifying the control effort to achieve a feasible, finite-time convergence of the system states [21]. Nevertheless, the control chattering remains an obstacle to the practical application of TSM. The higher-order sliding mode (HOSM) control system has been demonstrated to eliminate the chattering effect by concealing the high-frequency switching within the higher derivatives of the sliding variable [22] and are not restricted by the relative degree of the system [23]. Recent research in the literature has yielded various chattering-free SMC solutions. For instance, an adaptive strategy that guarantees fast finite-time convergence while avoiding singularities in nonlinear systems was proposed in [24]. Subsequently, a second-order non-singular TSM controller featuring a hierarchical control structure and a linear integral sliding variable was developed in [25]. Concurrently, a PID-type integral TSM manifold incorporating an inverse hyperbolic tangent function was introduced in [26] to eliminate chattering. The implementation of an extended state observer (ESO) has been demonstrated to be an effective method for compensating for nonlinear uncertainties and other disturbances, thereby further reducing chattering [27]. Regarding DPF regeneration temperature control, a study in the literature [20] proposed a composite control strategy that combines second-order TSM with an error-based ESO. This strategy not only ensures finite-time convergence and inherent chattering elimination but also demonstrates superior performance with more rapid disturbance rejection and more precise temperature tracking.

Motivated by the foregoing discussion, this study aims to develop a robust and practical strategy for DOC outlet temperature disturbance rejection control for efficient and reliable DPF thermal regenerations, with the primary objectives of achieving precise temperature tracking, eliminating control chattering and enhancing system robustness against disturbances. For this purpose, this paper carried out the design and evaluation of a novel control strategy that integrates the linear ESO (LESO), the chattering-free terminal sliding mode (CTSM), and the feedforward compensation (FFC). Its novelty and major contributions include the following: (i) The LESO design is based on the active disturbance

control (ADRC) framework. The lumped disturbance of the system, i.e., the total disturbance, is consequently accurately estimated. Its effect can then be timely compensated for in the control. (ii) The CTSM controller is designed by means of integrating a PID-type sliding variable with a non-singular TSM manifold through the second-order sliding mode technique. Therefore, it ensures a finite-time convergence of the sliding mode dynamics and a continuous, chattering-free control input. (iii) The introduction of the FFC further reduces the burden on the LESO and consequently enhances the system's capacity to reject high-frequency dynamic disturbances in practical applications. (iv) A composite control strategy is proposed by combining the LESO, the CTSM, and the FFC to ensure an effective regeneration temperature control in the work. The stability of the closed-loop system is proved by using the Lyapunov method. Its superior performance with respect to set-point tracking and disturbance rejection is verified in a high-fidelity GT-Power/MATLAB environment through a comprehensive co-simulation study.

The structure of this paper is arranged as follows. Section 2 formulates the DOC thermal dynamic model and clarifies the control problem. Section 3 details the design of the composite control strategy. Section 4 presents the simulation results and discussion. Section 5 summarizes the conclusions.

2. DOC Thermal Dynamics and Problem Formulation

As illustrated in Figure 1, the DOC is normally equipped right after the turbine of the engine in the exhaust line of modern diesel vehicles. It is of flow-through design and generally consists of ceramic substrate, washcoat, and noble metal catalyst. As shown in Figure 1, the catalyst is used to facilitate the hydrocarbon oxidation reaction occurred in the DOC. This catalytic reaction is an exothermic process and a lot of heat is thereby released, which facilitates the thermal regeneration process of the downstream DPF. During this process, the accumulated soot in the filter is oxidized and converted into CO_2 and water, once the temperature of the exhaust gas at the DOC outlet rises and maintains above 500 °C. To promote soot combustion in the filter, the engine control unit (ECU) periodically introduces an additional amount of fuel, either via in-cylinder post-injection or by direct injection into the exhaust line through a hydrocarbon doser installed right at the DOC inlet. Therefore, it is obvious that this extra amount of fuel injection/dosing should be carefully designed to maintain a reasonable and accurate thermal regeneration temperature T at the outlet of the DOC, despite the DOC inlet gas temperature T_0, the varying engine-out gas flow F, and other various internal and external disturbances as depicted in [14] in real applications.

It is seen that, during the thermal regeneration of DPF, the DOC can be treated as a single-input single-output (SISO) system from the point of view of control. The system input is the additional amount of fuel that is scheduled by the ECU, and the system output is the exhaust gas temperature T at the DOC outlet. Nevertheless, the inherent complexity of the DOC system is characterized by the presence of intricate chemical and thermal dynamics [16,20]. To facilitate control design, it has been reported recently that thermal dynamics of the DOC under steady-state engine operation conditions can be represented by a group of second-order transfer functions, which is expressed by [28]:

$$G(s) = \frac{K}{T_w^2 s^2 + 2\xi T_w s + 1} \tag{1}$$

where T_w is the time constant, s is the Laplace operator, ξ is the damping ratio, and K is the gain coefficient. Values of the model coefficients vary within a specific range and can be identified through experimental measurements. As in the literature [28], it is shown that the range of ξ is from 0.75 to 1.5 and that of T_w is from 6 to 32 over a wide engine

operating speed and load, which indicates that the DOC system is characterized by its slow temperature response during the regeneration process.

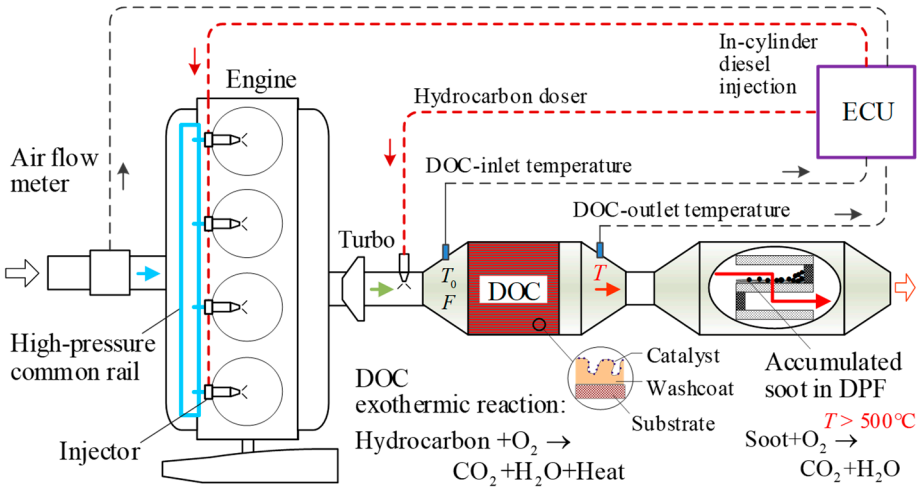

Figure 1. Schematic diagram of the DOC system in diesel engine exhaust line during DPF thermal regeneration.

Therefore, in view of the inevitable disturbances in practice, the thermal dynamics model of the DOC system can be formulated as:

$$\ddot{y}(t) = -a_1\dot{y}(t) - a_0 y(t) + bu(t) + d(t) \tag{2}$$

where t denotes time, $u(t)$ refers to the extra fuel or hydrocarbon flow rate at the DOC inlet that is also the system input, the system output $y(t)$ is defined as the DOC outlet temperature T, $d(t)$ denotes the inevitable external disturbances and unmodeled dynamics, a_1 and a_0 are the system parameters with $a_1 = 2\xi {T_w}^{-1}$ and $a_0 = {T_w}^{-2}$, and b is the control input gain with $b = K{T_w}^{-2}$.

The total disturbance term $f(t)$, which includes both internal model uncertainties and external unknown disturbances, is defined as:

$$f(t) = -a_1\dot{y}(t) - a_0 y(t) + (b - b_n)u(t) + d(t) \tag{3}$$

where b_n is the nominal value of the input gain b. Consequently, the state-space model of the DOC system can be further expressed as follows:

$$\begin{cases} \dot{x}_1(t) = x_2(t) \\ \dot{x}_2(t) = f(t) + b_n u(t) \\ y(t) = x_1(t) \end{cases} \tag{4}$$

where $[x_1,\ x_2]^T$ is the state vector and $[x_1,\ x_2]^T = \left[T,\ \dot{T}\right]^T$. For convenience, the following assumption is provided.

Assumption 1. *The total disturbance term f(t) is differentiable with respect to time, and f(t) and its derivative* $\dot{f}(t)$ *are both bounded.*

To achieve an efficient and reliable regeneration, the core challenge of the control problem is to guarantee that the system output $y(t)$ accurately tracks the desired trajectory in the presence of unmodelled dynamics, unpredictable external disturbances, and parameter uncertainties during the thermal regeneration process. Therefore, it is expected that the total disturbance $f(t)$ is timely estimated in run time; and the control input $u(t)$ is required

to be well designed and synthesized meticulously to ensure the requisite performance and robustness against both internal and external disturbances. In order to achieve the objective, a composite robust control scheme is devised in the following section.

3. Control Method

3.1. Linear Extended State Observer

Let $x_3(t) = f(t)$ denote an extended state of the DOC system (4) and $g(t) = \dot{f}(t)$. The preceding Equation (4) of the DOC system is rewritten as:

$$\begin{cases} \dot{x}_1(t) = x_2(t) \\ \dot{x}_2(t) = x_3(t) + b_n u(t) \\ \dot{x}_3(t) = g(t) \end{cases} \tag{5}$$

According to the literature [17], the linear extended state observer (ESO) of the DOC system can be designed as follows:

$$\begin{cases} \dot{\hat{x}}_1 = \hat{x}_2 + 3\omega_o(x_1 - \hat{x}_1) \\ \dot{\hat{x}}_2 = \hat{x}_3 + b_n u + 3\omega_o^2(x_1 - \hat{x}_1) \\ \dot{\hat{x}}_3 = \omega_o^3(x_1 - \hat{x}_1) \end{cases} \tag{6}$$

where $\hat{x}_i (i = 1, 2, 3)$ are the estimates of x_i and ω_o represents the bandwidth of the linear ESO and $\omega_o > 0$.

Define $\widetilde{x}_i = x_i - \hat{x}_i (i = 1, 2, 3)$ as the state estimation errors and subtract Equation (6) from Equation (5). It then leads to

$$\begin{bmatrix} \dot{\widetilde{x}}_1 \\ \dot{\widetilde{x}}_2 \\ \dot{\widetilde{x}}_3 \end{bmatrix} = \begin{bmatrix} -3\omega_o & 1 & 0 \\ -3\omega_o^2 & 0 & 1 \\ -\omega_o^3 & 0 & 0 \end{bmatrix} \begin{bmatrix} \widetilde{x}_1 \\ \widetilde{x}_2 \\ \widetilde{x}_3 \end{bmatrix} + \begin{bmatrix} 0 \\ 0 \\ 1 \end{bmatrix} g(t) \tag{7}$$

Lemma 1 [29]. *Assuming that $g(t)$ is bounded, there exists a finite time $t_i > 0$ and a positive constant γ_i so that*

$$\left|\widetilde{x}_i\right| \leq \gamma_i, \qquad i = 1, 2, 3, \forall t \geq t_i > 0 \tag{8}$$

holds. Furthermore, $\gamma_i = O(\frac{1}{\omega_o{}^k})$ for some positive integer k.

The above Lemma 1 has been proved by the literature [29]. As shown in Equation (8), it can be seen that the errors in state estimation decrease as the bandwidth of the linear ESO increases. Generally, the larger the observer bandwidth ω_o, the smaller the estimation errors $\left|\widetilde{x}_i\right|$. It has been established that the extended state x_3 in Equation (5) is introduced to denote the lumped term $f(t)$. In view of the preceding Assumption 1, it can be observed that, by selecting a proper bandwidth ω_o as in Equation (6), an accurate estimation of the bounded total disturbance $f(t)$ can be achieved. Therefore, the linear ESO (6) provides an effective way of reducing the complexity caused by unknown external disturbances, uncertain system dynamics, and the nonlinearity of the system. A more robust control performance with higher control accuracy can thus be obtained by applying $\hat{x}_3$ to compensate for and consequently alleviate the effect of the lumped total disturbance $f(t)$.

It is seen in Lemma 1 that the total disturbance term $f(t)$ can be accurately estimated and in Assumption 1 that the first derivative of $f(t)$, i.e., $g(t)$, is bounded. Therefore, the following assumption can be introduced to facilitate the subsequent control design.

Assumption 2. *The first time derivative of the estimation error* $\widetilde{x}_3$ *is bounded. That is,* $|\dot{\widetilde{x}}_3| = |\dot{x}_3 - \dot{\hat{x}}_3| = |\dot{f}(t) - \dot{\hat{x}}_3| \leq \delta$, *where* $\delta > 0$ *is a constant.*

3.2. Chattering-Free Terminal Sliding Mode Control

A chattering-free terminal sliding mode control is designed by using the second-order sliding mode technique in this section. First, define the reference temperature tracking error as:

$$e(t) = x_{1r}(t) - x_1(t) \tag{9}$$

where $x_{1r}(t)$, $x_1(t)$ are the reference and actual regeneration temperature, respectively.

A sliding variable of proportional–integral–derivative (PID) type is subsequently proposed for the thermal dynamics of the DOC system (5), as follows:

$$l(t) = \dot{e}(t) + k_1 e(t) + k_2 \int_0^t e(\tau) d\tau \tag{10}$$

where k_1 and k_2 are constant control gains with $k_1 > 0$ and $k_2 > 0$. The two control gains should be selected properly to guarantee that the characteristic polynomial $\lambda(s) = s^2 + k_1 s + k_2$ is strictly Hurwitz stable. That is, $k_1^2 - 4k_2 \geq 0$.

In order to guarantee $l(t)$ a finite-time convergence to zero, the non-singular TSM manifold is designed as in [30]:

$$\sigma(t) = l(t) + \beta^{-1} \dot{l}^{p/q}(t) \tag{11}$$

where p, q are both odds and $1 < p/q < 2$, and $\beta > 0$ is a constant.

Therefore, it can be seen that a specific control law for the DOC system (5) needs to be appropriately designed such that $l(t)$ and $\dot{l}(t)$ can be driven towards and maintained at $\sigma(t) = 0$ to achieve the nonlinear sliding mode motion. With $\sigma(t) = 0$, $l(t)$ will reach and be kept at zero in a finite time according to the literature [30]. In view of Equation (10), when $l(t) = 0$ is reached, the temperature error $e(t)$ will converge to zero asymptotically.

Theorem 1. *For the system described by Equation (5) along with the sliding function (10) and the second-order non-singular TSM manifold (11), the temperature tracking error (9) converges to zero asymptotically if the designed control law is as follows:*

$$u(t) = \frac{u_R(t) + u_L(t)}{b_n} \tag{12}$$

with

$$u_R(t) = \ddot{x}_{1r} + k_1 \dot{e} + k_2 e + \frac{\beta q}{p} \int_0^t \dot{l}^{2-(p/q)}(\tau) d\tau + \eta \int_0^t \mathrm{sgn}(\sigma(\tau)) d\tau \tag{13}$$

$$u_L(t) = -\dot{\hat{x}}_3 \tag{14}$$

where $\eta > 0$ *is a positive constant.*

Proof of Theorem 1. To demonstrate the stability of the designed control law, consider the following Lyapunov function:

$$V(t) = \frac{1}{2}\sigma^2(t) \tag{15}$$

Consequently,

$$\dot{V}(t) = \sigma(t)\dot{\sigma}(t) \tag{16}$$

Taking the time derivatives of Equations (11) and (10) and considering the thermal dynamics (5), it then leads to

$$\begin{aligned}\dot{V}(t) &= \sigma(t)\left(\tfrac{p}{\beta q}\dot{l}^{(p/q)-1}(t)\ddot{l}(t) + \dot{l}(t)\right) \\ &= \sigma(t)\tfrac{p}{\beta q}\dot{l}^{(p/q)-1}(t)\left(k_1\ddot{e} + k_2\dot{e} + \tfrac{d}{dt}(\ddot{x}_{1r} - x_3 - b_n u(t)) + \tfrac{\beta q}{p}\dot{l}^{2-(p/q)}(t)\right)\end{aligned} \tag{17}$$

Substituting the control law Equation (12) into Equation (17) yields the following result:

$$\begin{aligned}\dot{V}(t) &= \sigma(t)\tfrac{p}{\beta q}\dot{l}^{(p/q)-1}(t)\left(-(\dot{x_3} - \dot{\hat{x}}_3) - \eta\mathrm{sgn}(\sigma(t))\right) \\ &= \tfrac{p}{\beta q}\dot{l}^{(p/q)-1}(t)\left(-\dot{\tilde{x}}_3\sigma(t) - \eta\left|\sigma(t)\right|\right)\end{aligned} \tag{18}$$

Define $\theta = -\delta + \eta$ and $\theta > 0$. Considering Assumption 2, one has

$$\begin{aligned}\dot{V}(t) &\le \tfrac{p}{\beta q}\dot{l}^{(p/q)-1}(t)(\left|\dot{\tilde{x}}_3\right||\sigma(t)| - \eta|\sigma(t)|) \\ &\le -\theta\tfrac{p}{\beta q}\dot{l}^{(p/q)-1}(t)|\sigma(t)|\end{aligned} \tag{19}$$

since p, q are odds and $1 < p/q < 2$ such that $\dot{l}^{(p/q)-1}(\mathrm{t}) \ge 0$ holds.

Let $\rho(t) = \theta\frac{p}{\beta q}\dot{l}^{(p/q)-1}(t)$. The above Equation (19) is rewritten as

$$\dot{V}(t) \le -\rho(t)|\sigma(t)| = -\sqrt{2}\rho(t)V^{1/2} \tag{20}$$

Therefore, it is seen that, for the case $\dot{l}(t) \neq 0$, i.e., $\rho(t) \neq 0$, the time derivative of the selected Lyapunov function (15) is negative definite. According to the literature [30], the nonlinear sliding mode motion $\sigma(t) = 0$ is then reached in a finite time t_r such that

$$t_r \le \sigma(0)/\rho(0) \tag{21}$$

For the case when $\dot{l}(t) = 0$, i.e., $\rho(t) = 0$, by combining the control law (12) along with several basic algebraic operations, it can be deduced that:

$$\begin{aligned}\ddot{l}(t) &= -(\dot{x_3} - \dot{\hat{x}}_3) - \eta\mathrm{sgn}(\sigma(t)) \\ &= -\dot{\tilde{x}}_3 - (\delta + \theta)\mathrm{sgn}(\sigma(t))\end{aligned} \tag{22}$$

It can be observed that the above Equation (22) leads to $\ddot{l}(t) \le -\theta < 0$ for $\sigma(t) > 0$, and $\ddot{l}(t) \ge \theta > 0$ for $\sigma(t) < 0$. So, the case $\dot{l}(t) = 0$ (but $l(t) \neq 0$) is not an attractor, as is also shown in [30]. Consequently, it is concluded that the nonlinear sliding mode motion $\sigma(t) = 0$ can be reached within finite time and guarantees the Lyapunov stability condition. As in the literature [30], the linear sliding mode motion $l(t) = 0$ will be reached in a finite time after $\sigma(t) = 0$. With $l(t) = 0$, it is evident that the temperature tracking error $e(t)$ will asymptotically converge to zero in view of Equation (10), as long as the control gains are designed as $k_1 > 0$, $k_2 > 0$, and $k_1^2 - 4k_2 \ge 0$ to make $\lambda(s) = s^2 + k_1 s + k_2$ Hurwitz. This ends the proof. □

It is notable that $\ddot{x}_{1r}$ is required in the designed control Equation (12). This is applicable as the reference temperature is usually predetermined during the thermal regeneration process [31]. In addition, it can be seen in Equations (12) and (13) that the conventional switching term of sliding mode control is smoothed by an integration operation. It conse-

quently leads to an inherently continuous control action. Therefore, it is evident from the presented control design that both finite-time convergence and a chattering-free control are achieve through the combination of a PID-type sliding variable with a non-singular TSM manifold within the second-order sliding mode framework. Furthermore, it is observed in Theorem 1 and its proof above that a more robust control is obtained by combining the estimated total disturbance $\hat{x}_3$ produced by the preceding linear ESO as in Equation (6). Consequently, it implies that only a moderate value of η is needed to avoid undesired chattering or overshoot effects. The primary advantage of the proposed control is its ability to deliver robust and rapid performance in the face of varying internal uncertainties and external disturbances. This is beneficial for an efficient and reliable thermal regeneration process.

3.3. Feedforward Compensation

During real-world driving cycles, the DPF regeneration often occurs under transient engine conditions with constantly varying exhaust gas flow and temperature. In this section, a feedforward compensation (FFC) scheme is designed based on the measured DOC inlet gas temperature T_0 and exhaust mass flow rate F. From a control perspective for DOC system, both T_0 and F can be regarded as the external disturbances. Therefore, their effects can be immediately compensated for in the FFC path, thereby reducing the burden of the pre-designed linear ESO. This is beneficial to achieving a better performance. The FFC scheme is designed based on the principle of conservation of energy and is expressed as follows [14]:

$$FC_p(x_{1r} - T_0) = \eta_c u_F q_{LHV} \tag{23}$$

where F is the measured mass flow rate, T_0 is the DOC inlet gas temperature, C_p is the specific heat capacity of the exhaust gas, u_F is the control effort of the FFC, η_c is the conversion efficiency of the DOC, and q_{LHV} refers to the lower heating value of diesel fuel.

Denoting $\zeta = x_{1r}/T_0$ with $\zeta \geq 1$, the above Equation (23) is rewritten as:

$$u_F = K_F F \tag{24}$$

where $K_F = C_p T_0(\zeta - 1)/(\eta_c q_{LHV})$.

To summarize, the foregoing design of the proposed control scheme is shown in Figure 2. It is seen that a composite control scheme is obtained by combining the linear ESO as in (6), the chattering-free TSM as in (13) and the FFC as in (24) to ensure an effective regeneration temperature control in the work. Obviously, the introduction of the FFC does not affect the stability of the closed-loop control system. By applying the FFC, the effect of disturbances caused by the exhaust gas variations at the DOC inlet is timely compensated for. As a result, the burden of the linear ESO is significantly alleviated, thus facilitating enhanced control performance in view of Equation (13).

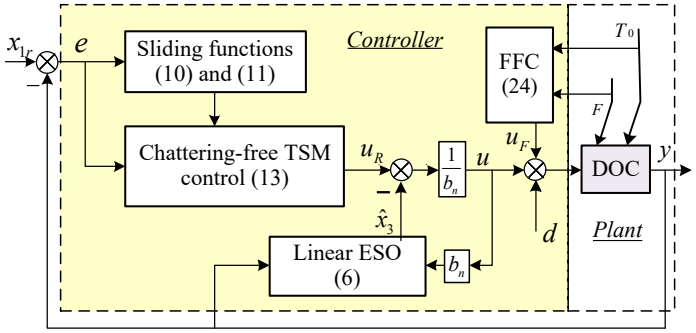

Figure 2. Block diagram of the proposed composite and robust temperature control scheme.

4. Simulation Results and Discussion

In order to evaluate the performance of the designed control, a co-simulation environment was established by using GT-Power and MATLAB as depicted in Figure 3 in the work. The versions of the MATLAB and GT-Power software were 2024b and v2016, respectively. The one-dimensional (1D) integrated GT-power model, which consists of the engine, vehicle, driver controls, and the aftertreatment system, was provided by Gamma Technologies for the purpose of testing and validating different drive cycles with steady-state and transient engine operation conditions. The engine component was based on a 2.0 L turbo-charged diesel engine. The driver provides the runtime accelerator and gear positions for the engine and vehicle, respectively. In addition, a high-fidelity 1D DOC model was provided for the purpose of studying the effects of catalyst loading, DOC sizing, and the DOC conversion efficiency in the aftertreatment system. The high-fidelity DOC model was developed based on the literature [32], with its major specifications listed in Table 1. In the aftertreatment system (as in Figure 3), the aftertreatment control unit (ACU) represents the proposed controller designed in the previous Section 3 for DOC outlet temperature control during the thermal regeneration of DPF. The preceding design of the control scheme is implemented in MATLAB/Simulink so that a closed-loop co-simulation is achieved.

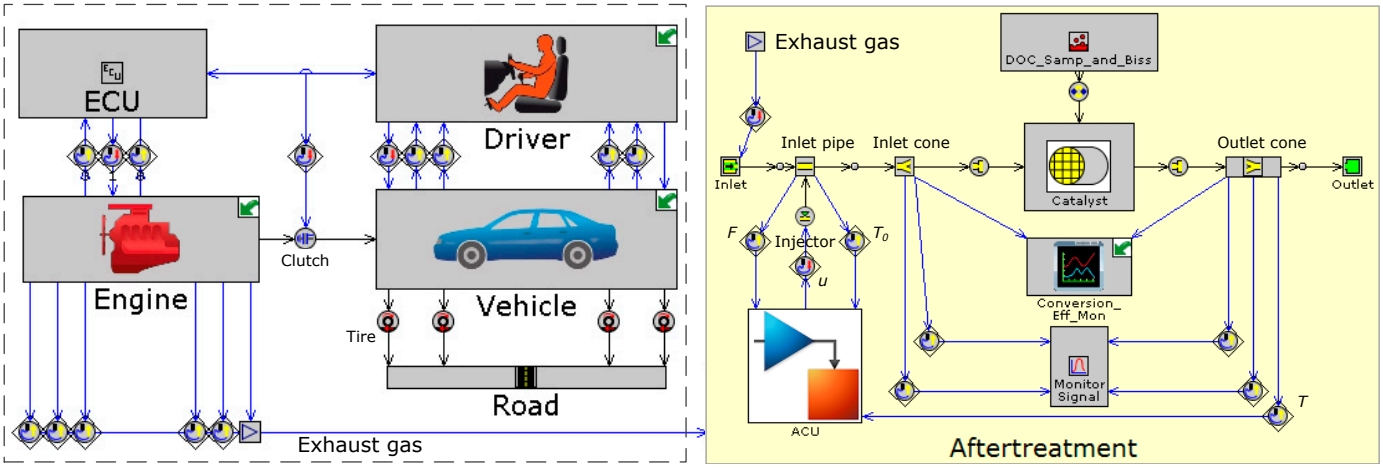

Figure 3. The co-simulation environment established via GT-Power and MATLAB/Simulink.

Table 1. Specifications of the GT-Power high-fidelity 1D DOC model.

Substrate	Cordierite
Catalyst	PGM
Frontal area (mm^2)	20,000
Length (mm)	160
Cell density (cpsi)	400
Substrate density (kg/m^3)	1720

A step response test under a typical medium engine operation condition is first carried out through manually scheduling a step change of the control input $u(t)$ in the co-simulation environment, where a step-change amount of the hydrocarbon dosing rate in the range of 0.15–0.25 g/s is injected into the exhaust pipe. Consequently, as presented in Figure 4, the 1D DOC model produces an increase in temperature of about 75 °C at the

DOC outlet. The step-change temperature profile can be identified by a linear second-order transfer function model as follows by using the system identification toolbox in MATLAB:

$$G(s) = \frac{727.68}{237.42s^2 + 22.37s + 1} \tag{25}$$

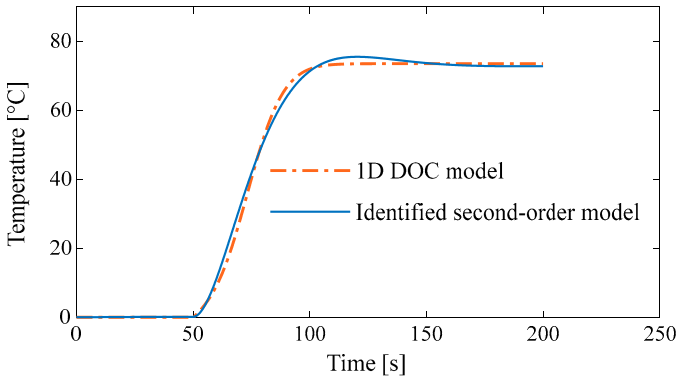

Figure 4. Step responses of the DOC outlet temperature by the 1D DOC model and the identified second-order model.

The identified second-order transfer function model (25) has a fitting accuracy of 95.78% and its step response of temperature profile is also presented in Figure 4. It can be seen that the outputs of the identified second-order model and the high-fidelity 1D DOC model match fairly well. Thus, the nominal value of the control input gain can be obtained as $b_n = 3.06$ in view of the Equations (4) and (25).

4.1. Parameter Selection

The other control gains are tuned by using the identified second-order model as in Equation (25) and adjusted in MATLAB/Simulink by means of simulation. The selection of the TSM parameters has been discussed extensively in the literature; so, they were selected as $p/q = 1.4$ and $\beta = 0.03$ according to the guidelines in [20] and in [30]. The control gains k_1 and k_2 as in Equation (10) need to be selected properly to make $\lambda(s) = s^2 + k_1 s + k_2$ Hurwitz as was aforementioned. It is also seen in the robust control as in Equation (13) that the larger the gain k_2, the faster the response speed. However, values of k_1 and k_2 that are too large may lead to undesirable temperature overshoot. Hence, the control gains k_1 and k_2 were tuned by trial-and-error methods and their final values were selected as $k_1 = 0.06$ and $k_2 = 0.000012$ for a sensible trade-off between performance and robustness of the control. For the control gain η, it is selected as $\eta = 0.02$ to guarantee the Lyapunov stability of the close-loop system. Based on these tuned gain parameters, Figure 5 shows the simulation results of a reference step response by using the chattering-free TSM control as in Equation (13) and second-order model as in Equation (25), where the sampling time interval was selected as 0.01 s. It can be seen that the actual temperature is capable of tracking the reference and no significant chattering in the control input signal occurs. In Figure 5a, it is also shown that the control input $u(t)$ has only a small oscillation magnitude of less than 0.0002 g/s, attributed to the utilization of the second-order sliding mode.

The tuning of the observer bandwidth ω_o is similar to that of literature [33,34]. A moderate value of 0.25 was selected. Figure 6 show the simulation results by using the identified second-order model as in Equation (25) and the designed control law as in Equation (12), where a step change of the reference temperature from 500 to 600 °C occurs at the beginning of the simulation and then after t = 300 s the external disturbance $d(t)$ with a magnitude of 0.6 is introduced as in Figure 6b. The extended state $x_3(t)$ is calculated by Equation (3), representing the total disturbance term $f(t)$. It is demonstrated that the linear

ESO performs well and all the system states can be timely and accurately estimated even in the presence of sharp disturbances and reference-step change.

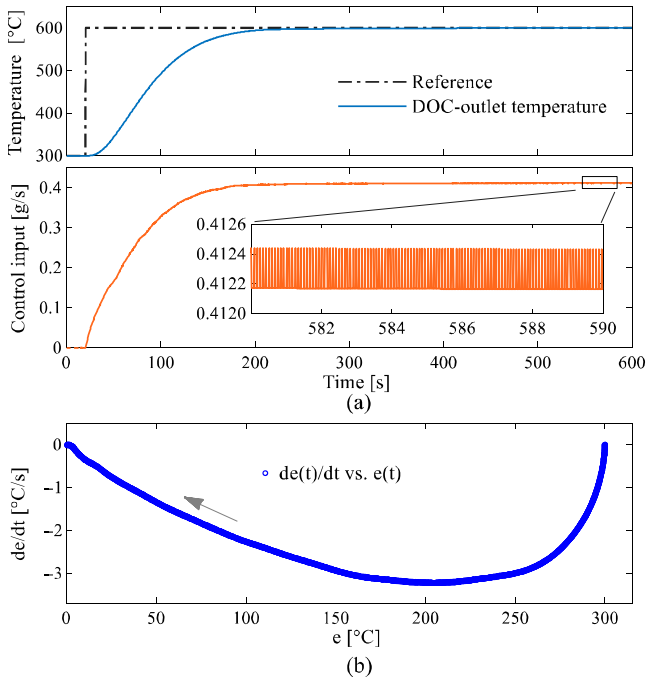

Figure 5. Simulation results under a reference-step response of the chattering-free TSM controller. (**a**) Temperature control results along with the control input $u(t)$. (**b**) Results of phase-plane plot of the temperature tracking errors, i.e., $\dot{e}(t)$ versus $e(t)$.

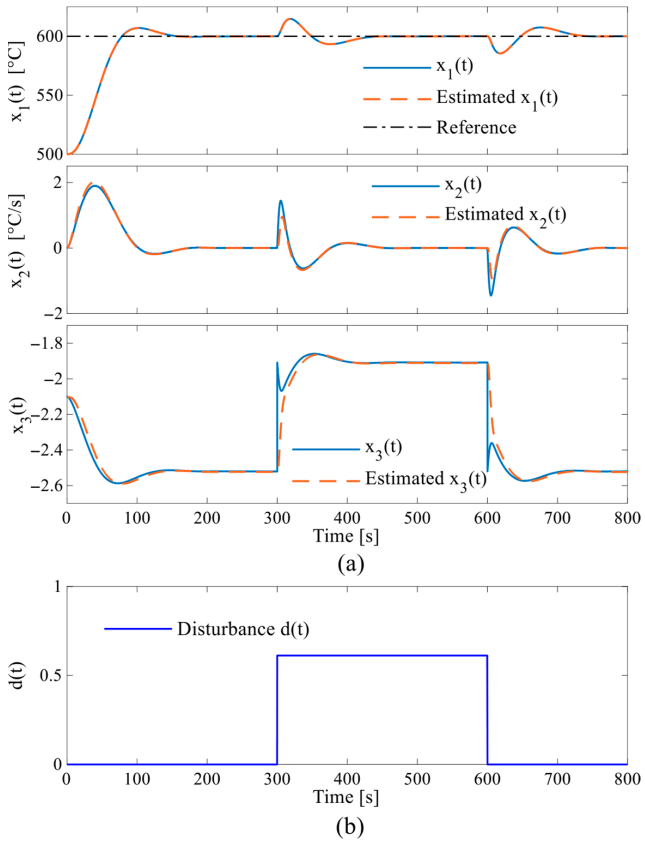

Figure 6. Simulation results of the linear ESO performance. (**a**) Results of the system states and their estimation. (**b**) The introduced disturbance term $d(t)$.

An overview of the well-tuned control parameters is presented in Table 2. To perform a comparative analysis, three different controller configurations were implemented, and their results were analyzed and discussed in the following simulation study. That is,

Table 2. Control parameters of the developed composite controller.

ω_o	k_1	k_2	p	q	β	η
0.25	0.06	0.000012	7	5	0.03	0.02

(1) CTSM: This refers to the chattering-free TSM control scheme in Section 3.2, and the $u_R(t)$ in Equation (13) is used as the only control effort applied to the 1D DOC model.
(2) CTSM-LESO: The CTSM controller and the linear ESO are combined for a more robust disturbance compensation, where $u(t)$ in Equation (12) is implemented as the final control effort towards the 1D DOC model.
(3) CTSM-LESO-FFC: The FFC is introduced and integrated with the aforementioned CTSM-LESO controller. This combination scheme is demonstrated in Figure 2, where u_F and u are added together to serve as the final control effort.

In addition, the controller that combines CTSM and FFC (denoted as CTSM-FFC) is also implemented for a more comprehensive investigation in the study. The sampling time for each implemented controller was 0.01 s and the gas temperature at the DOC inlet was selected as 375 °C in the simulation tests.

4.2. Set-Point Tracking Performance

In order to guarantee a reliable regeneration, the reference temperature varies accordingly during different stages of the thermal regeneration process [20]. The results of temperature profiles in relation to set-point tracking along with the control input $u(t)$ produced by each controller are presented in Figure 7, where the reference temperature varies between 400 and 600 °C and the temperature rising or falling rate is 10 °C/s. The simulation tests were carried out under a typical steady-state engine operating condition with constant exhaust gas mass flow of 200 kg/h.

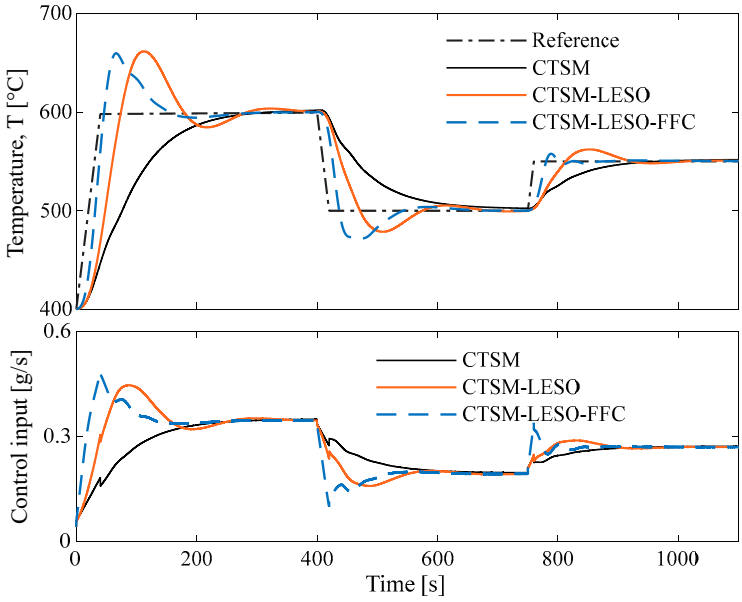

Figure 7. Control performance of CTSM, CTSM-LESO, and CTSM-LESO-FFC in relation to set-point tracking.

In Figure 7, it is shown that all the controllers achieve the desired temperature. Furthermore, the chattering phenomenon, which exhibits high-frequency oscillation in the control action in conventional SMC, is eliminated in the proposed control scheme, as previously discussed. A chattering-free, continuous control input is generated by each implemented controller, as shown in Figure 7. Among these controllers, the CTSM produces no temperature overshoot but at the cost of the largest rise time. By introducing the linear ESO to estimate the total disturbance, the CTSM-LESO timely compensates for its effect and produces a much faster temperature response since the rise time is much less than that of the CTSM. However, it is at the cost of a slightly larger temperature overshoot. In real applications, this temperature overshoot can be reduced by selecting an appropriate reference rise rate as in [31]. The CTSM-LESO-FFC shows a similar overshoot to the CTSM-LESO, but features a substantially reduced rise and settling time. Therefore, it can be noted that the CTSM-LESO-FFC achieves the best performance among the three controllers with respect to set-point tracking. The same result can also be obtained from Figure 8, since the CTSM-LESO-FFC provides the least amount of integral absolute error (IAE) among the three controllers during the simulation tests, where the IAE is defined as IAE = $\int_0^t |e(\tau)|d\tau$.

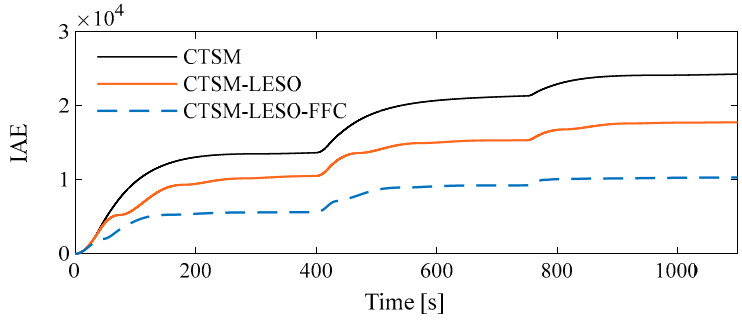

Figure 8. IAE of CTSM, CTSM-LESO, and CTSM-LESO-FFC in relation to set-point tracking.

4.3. Performance Under Step-Change Disturbances

In real applications, the DOC system usually experiences various external disturbances during the thermal regeneration process, such as the occasional failure of the hydrocarbon doser and the high frequency variation in the exhaust flow. Figure 9 demonstrates the temperature control results under a disturbance step-change, where a certain amount of disturbance $d(t)$ is introduced at t = 50 s (as in Figure 9b) to simulate the doser failure. The tests were conducted under a standard steady-state engine operating condition, where the reference temperature remained 600 °C and the exhaust gas mass flow was constant 200 kg/h. Obviously, it is shown in Figure 9a that the CTSM and the CTSM-FFC produces the largest overshoot and the longest settling time among the four controllers. A better temperature response is obtained by the CTSM-LESO and CTSM-LESO-FFC due to the effectiveness of the linear ESO. As can be seen from Figure 9b, the introduced $d(t)$ is timely estimated by both CTSM-LESO and CTSM-LESO-FFC. Its effect is then timely compensated for in the control of CTSM-LESO and CTSM-LESO-FFC, respectively. Therefore, more aggressive control inputs are produced by the CTSM-LESO and CTSM-LESO-FFC than those of the CTSM and CTSM-FFC as shown in Figure 9a. It is also noted that the objective of the developed FFC is to compensate for the effect of the variations in the exhaust gas flow and temperature in view of (24). The FFC u_F can thus be considered as a constant in the case of step change of $d(t)$, since the test is conducted at a steady engine state with a constant gas flow and temperature. Therefore, the CTSM and CTSM-FFC have similar temperature profiles and control inputs as in Figure 9a. The results of the CTSM-LESO-FFC and CTSM-LESO are similar to those of CTSM and CTSM-FFC. However, by introducing the FFC, the magnitude of the estimated total disturbance of CTSM-LESO-FFC is much reduced as

in Figure 9b. This is beneficial to the improvement in temperature control performance, especially in the presence of unknown external disturbances in real applications.

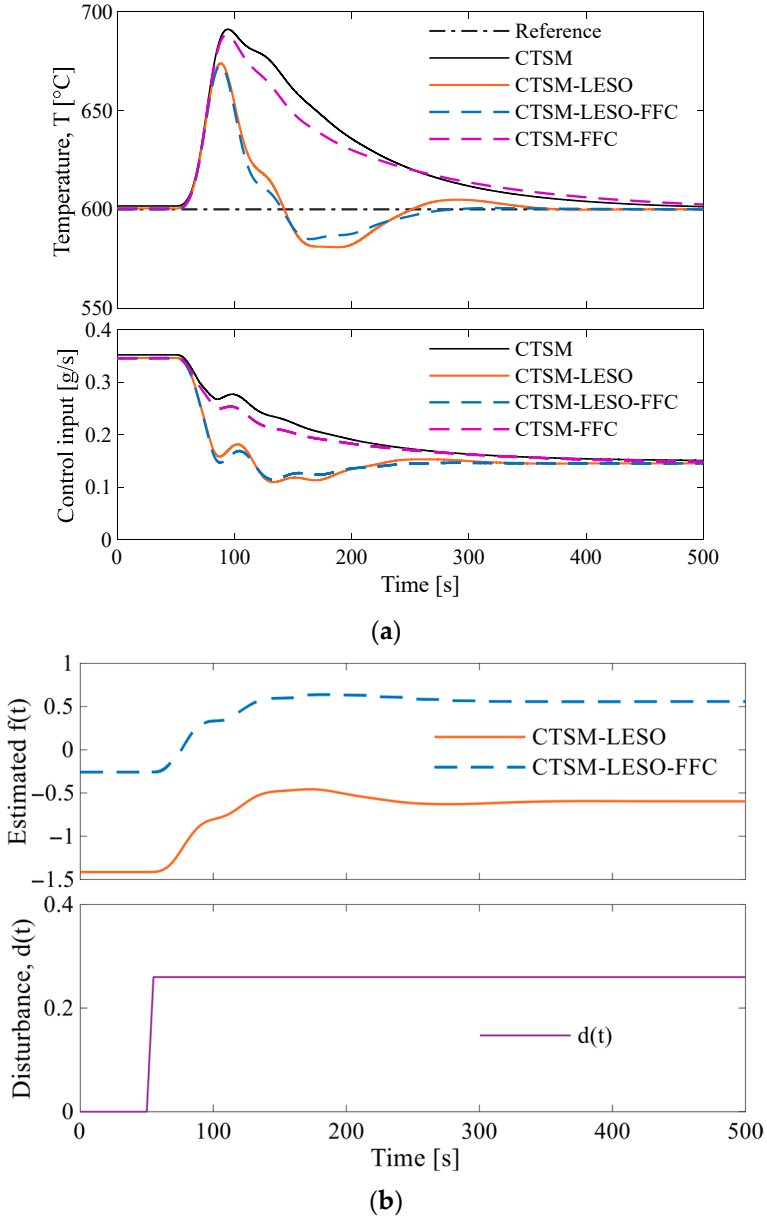

Figure 9. Temperature control performance of CTSM, CTSM-LESO, CTSM-LESO-FFC, and CTSM-FFC under the step change in disturbance $d(t)$. (**a**) Reference and actual temperature profiles and control inputs. (**b**) The step change of $d(t)$ and the estimated $f(t)$ of CTSM-LESO and CTSM-LESO-FFC.

In addition, simulation tests with respect to temperature control performance during the sudden changes in exhaust gas mass flow were also conducted. Figure 10 shows the results of temperature control performance for the exhaust mass flow rate sudden decrease in the range of 300–150 kg/h. Results of the temperature profiles and time trajectories of the control inputs are presented in Figure 10a; and the time history of the estimated total disturbance $f(t)$, the sliding function $l(t)$, and the sudden change in exhaust mass flow rate are presented Figure 10b. In Figure 11, the same results for the exhaust mass flow rate sudden increase in the range of 150–300 kg/h are presented. The reference temperature during the testing is constant at 600 °C. It is demonstrated in both Figures 10 and 11 that the CTSM-LESO-FFC achieves the best performance with the shortest settling time and least overshoot among the four controllers during the sudden change in exhaust mass

flow. Attributed to the effectiveness of the linear ESO, the CTSM-LESO produces a more aggressive control input and a faster temperature response than those of the CTSM. When the FFC is further introduced by the CTSM-LESO-FFC, it achieves a more rapid response to the sudden changes in exhaust mass flow rate in comparison to the CTSM-LESO. In the case of CTSM-FFC without the linear ESO, it can be seen in Figures 10a and 11a that the settling time becomes much longer compared to that of the CTSM-LESO-FFC. This can also be observed in both Figures 10b and 11b that the sliding function $l(t)$ of the CTSM-LESO-FFC takes the least convergence time among the four controllers. Moreover, it is seen in Figures 10b and 11b that the magnitude of the estimated total disturbance $f(t)$ is much reduced attributed to the introduction of FFC, which contributes to the temperature control performance in the presence of exhaust flow variations.

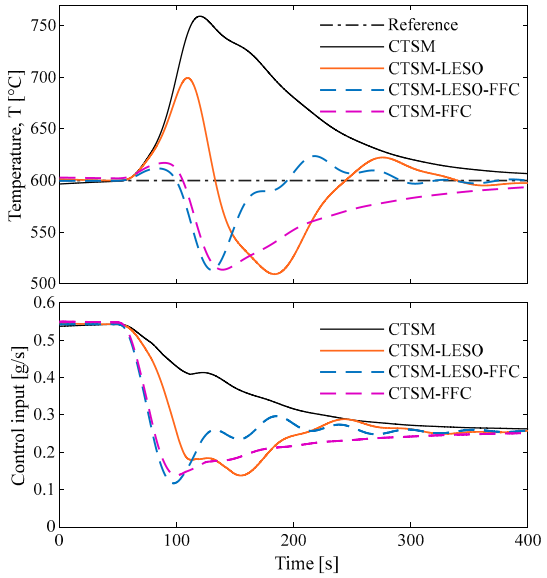

(**a**)

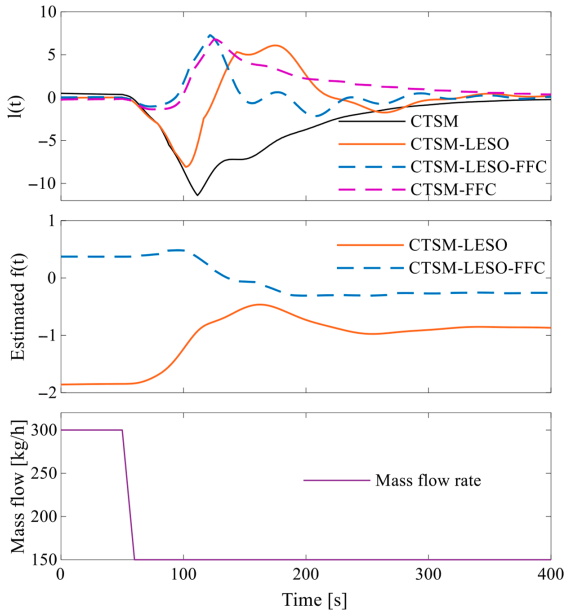

(**b**)

Figure 10. Temperature control performance of CTSM, CTSM-LESO, CTSM-LESO-FFC, and CTSM-FFC under the sudden decrease in exhaust mass flow in the range of 300–150 kg/h. (**a**) Reference and actual temperature profiles and control inputs. (**b**) Sliding function $l(t)$, estimated total disturbance $f(t)$, and the sudden change in exhaust mass flow rate.

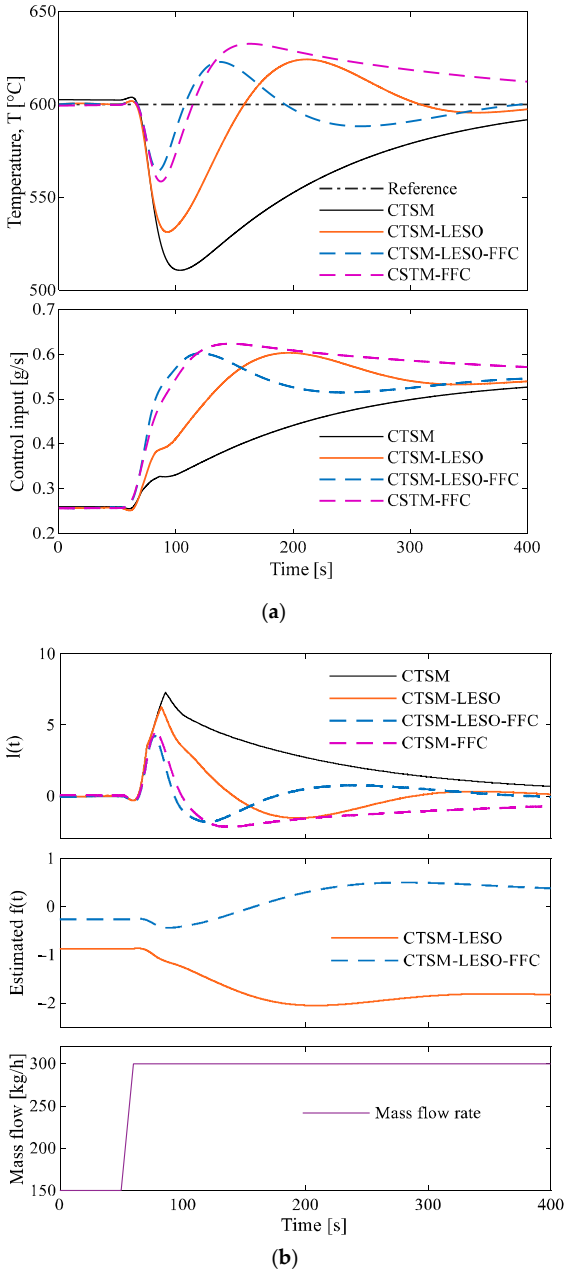

Figure 11. Temperature control performance of CTSM, CTSM-LESO, CTSM-LESO-FFC, and CTSM-FFC in the presence of exhaust mass flow rate sudden increase in the range of 150–300 kg/h. (**a**) Reference and actual temperature profiles and control inputs. (**b**) Sliding function $l(t)$, estimated total disturbance $f(t)$, and the sudden change in exhaust mass flow rate.

4.4. Performance Under NEDC Test Cycle

The foregoing results and discussions demonstrate clearly that the CTSM-LESO- FFC achieves superior temperature control performance with respect to disturbance rejection over the CTSM-FFC, CTSM-LESO, and CTSM. In this section, its control performance is further verified by applying the new European drive cycle (NEDC) established in the co-simulation environment. Figure 12 shows the high-frequency variations in both the engine speed and the exhaust mass flow rate under the NEDC test cycle. The significant and continued change in the engine operation conditions makes it rather difficult to control the regeneration temperature accurately in practical applications. In Figure 13, the results of temperature control performance of the CTSM-LESO-FFC under the NEDC cycle are demonstrated and compared with those of a modified ADRC (mADRC)-based composite

controller as developed in [16]. The reference temperature for both controllers during the testing is constant at 600 °C. It can be seen that both of the CTSM-LESO-FFC and mADRC-based controllers perform well under the NEDC test cycle as the actual temperature at the DOC outlet is maintained at nearly 600 °C. The temperature tracking error of both controllers is within the range of ±15 °C during the tests. However, the CTSM-LESO-FFC shows less temperature fluctuation under most conditions (as in Figure 13) and it produces much less IAE at the end of the NEDC test cycle than that of the mADRC-based controller. This demonstrates the effectiveness and superiority of the CTSM-LESO-FFC scheme proposed in this paper. Moreover, attributed to its ease of implementation, the proposed CTSM-LESO-FFC scheme can also be applied to other types of robust process control systems for improved performance.

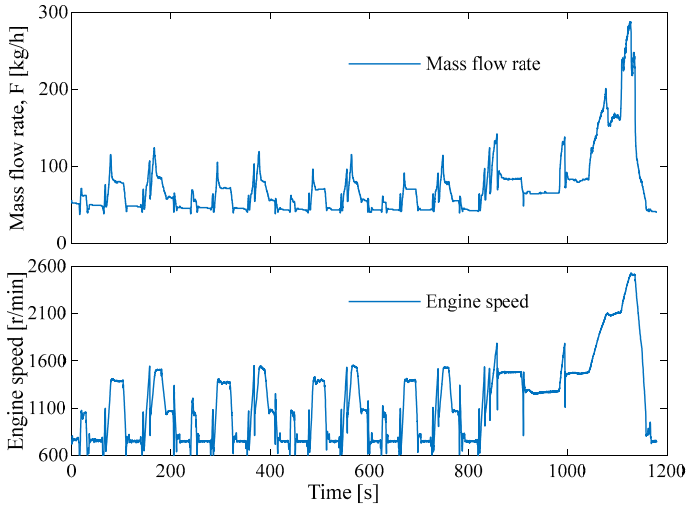

Figure 12. The exhaust mass flow rate and engine speed during the co-simulation under NEDC.

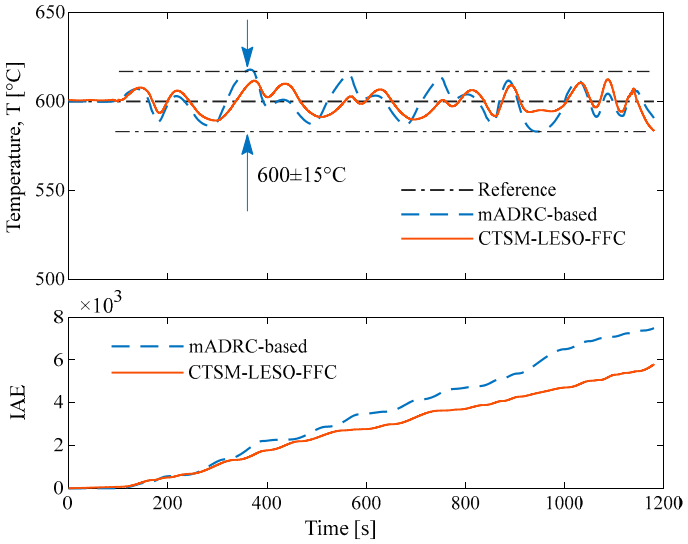

Figure 13. Temperature control performance of the CTSM-LESO-FFC and mADRC-based controllers under the NEDC test cycle.

5. Conclusions

To achieve an effective and dependable thermal regeneration in modern diesel vehicles, this paper successfully developed a novel composite control scheme for DOC outlet temperature control during the DPF thermal regeneration. The presented control is designed based on a representative, identified transfer function model of the plant system. Hence,

the nominal value of the input gain is the only parameter that is required. In addition, the chattering effect is significantly reduced by using a PID-type sliding variable and the second-order sliding mode technique. A chattering-free, continuous control input is thus produced. Moreover, the magnitude of the estimated total disturbance is further alleviated with the adoption of FFC based on energy conservation. A more robust temperature control performance is consequently achieved through combining the LESO, CTSM, and FFC. The stability of the proposed control design was proved in theory by using the Lyapunov approach. Its disturbance rejection performance was verified through comprehensive simulation studies by using a high-fidelity 1D DOC model built in GT-Power. The results demonstrate the effectiveness and superiority of the proposed CTSM-LESO-FFC scheme for reliable DOC-outlet temperature control during the thermal regeneration process. The control scheme can also be applied to other types of robust process control systems for improved performance due to its ease of implementation. In future study, a further investigation of the control strategy in real-time applications will be conducted to verify its consistent performance and robustness in the presence of measurement noises, unmodeled dynamics, and hardware limitations.

Author Contributions: Conceptualization, T.H. and X.C.; methodology, T.H., Q.J. and X.C.; software, T.H., Q.J. and X.C.; validation, T.H. and X.C.; formal analysis, T.H., X.C. and Q.J.; investigation, T.H., Q.J. and X.C.; resources, T.H. and X.C.; data curation, T.H., X.C. and Q.J.; writing—original draft preparation, T.H., X.C. and Q.J.; writing—review and editing, T.H.; visualization, X.C.; project administration, T.H.; funding acquisition, T.H. All authors have read and agreed to the published version of the manuscript.

Funding: This research was funded by the Beibu Gulf University Research Fund under grant 23KYQD39.

Data Availability Statement: The original contributions presented in this study are included in the article. Further inquiries can be directed to the corresponding author.

Conflicts of Interest: The authors declare no conflicts of interest.

References

1. Liu, Y.; Ge, Y.; Tan, J.; Wang, H.; Ding, Y. Research on ammonia emissions characteristics from light-duty gasoline vehicles. *J. Environ. Sci.* **2021**, *106*, 182–193. [CrossRef]
2. Piqueras, P.; García, A.; Monsalve-Serrano, J.; Ruiz, M.J. Performance of a diesel oxidation catalyst under diesel-gasoline reactivity controlled compression ignition combustion conditions. *Energy Convers. Manag.* **2019**, *196*, 18–31. [CrossRef]
3. Jin, N.; Long, W.; Xie, C.; Tian, H. After-Treatment Technologies for Emissions of Low-Carbon Fuel Internal Combustion Engines: Current Status and Prospects. *Energies* **2025**, *18*, 4063. [CrossRef]
4. Sun, H.; Liu, Y.; Li, N.; Tan, J. Study on Characteristics and Control Strategy of Diesel Particulate Filters Based on Engine Bench. *Processes* **2022**, *10*, 1246. [CrossRef]
5. Liu, G.; Liu, W.; He, Y.; Gong, J.; Li, Q. Research on Influence of Exhaust Characteristics and Control Strategy to DOC-Assisted Active Regeneration of DPF. *Processes* **2021**, *9*, 1403. [CrossRef]
6. Zhang, Z.; Dong, R.; Lan, G.; Yuan, T.; Tan, D. Diesel particulate filter regeneration mechanism of modern automobile engines and methods of reducing PM emissions: A review. *Environ. Sci. Pollut. Res.* **2023**, *30*, 39338–39376. [CrossRef]
7. Meng, Z.; Zeng, B.; Tan, J.; Chen, Z.; Ou, J. Study of gas and particulate emission characteristics during the fast regeneration period of DPF. *Fuel* **2022**, *317*, 123353. [CrossRef]
8. Huang, Y.; Ng, E.C.Y.; Surawski, N.C.; Zhou, J.L.; Wang, X.; Gao, J.; Lin, W.; Brown, R.J. Effect of diesel particulate filter regeneration on fuel consumption and emissions performance under real-driving conditions. *Fuel* **2022**, *320*, 123937. [CrossRef]
9. Wu, G.; Feng, G.; Li, Y.; Ling, T.; Peng, X.; Su, Z.; Zhao, X. A Review of Thermal Energy Management of Diesel Exhaust after-Treatment Systems Technology and Efficiency Enhancement Approaches. *Energies* **2024**, *17*, 584. [CrossRef]
10. Eck, C.; Nakano, F. Robust DPF Regeneration Control for Cost-Effective Small Commercial Vehicles. In *Proceedings of the 13th International Conference on Engines & Vehicles*; SAE Technical Paper; 2017-24-0123; SAE International: Warrendale, PA, USA, 2017. [CrossRef]

11. Dimaratos, A.; Giechaskiel, B.; Clairotte, M.; Fontaras, G. Impact of Active Diesel Particulate Filter Regeneration on Carbon Dioxide, Nitrogen Oxides and Particle Number Emissions from Euro 5 and 6 Vehicles under Laboratory Testing and Real-World Driving. *Energies* **2022**, *15*, 5070. [CrossRef]
12. Rsetam, K.; Al-Rawi, M.; Cao, Z. Robust adaptive active disturbance rejection control of an electric furnace using additional continuous sliding mode component. *ISA Trans.* **2022**, *130*, 152–162. [CrossRef]
13. Lepreux, O.; Creff, Y.; Petit, N. Model-based temperature control of a diesel oxidation catalyst. *J. Process Control* **2012**, *22*, 41–50. [CrossRef]
14. Huang, T.; Hu, G.; Meng, Z.; Zeng, D. IMC-based diesel oxidation catalyst outlet temperature control with extended state predictor observer. *Control Eng. Pract.* **2021**, *117*, 104939. [CrossRef]
15. Ning, J.; Yan, F. IMC based Iterative Learning Control of DOC Temperature during DPF Regerneration. In *Proceedings of the 2016 European Control Conference (ECC)*; IEEE: Piscataway, NJ, USA, 2016. [CrossRef]
16. Ning, J.; Yan, F. Disturbance rejection in DOC-out temperature control for DPF regeneration. *Proc. Inst. Mech. Eng. Part D J. Automob. Eng.* **2016**, *231*, 487–499. [CrossRef]
17. Huang, T.; Hu, G.; Yan, Y.; Zeng, D.; Meng, Z. Combined feedforward and error-based active disturbance rejection control for diesel particulate filter thermal regeneration. *ISA Trans.* **2023**, *134*, 28–41. [CrossRef]
18. Liu, W.; Gao, Y.; You, Y.; Jiang, C.; Hua, T.; Xia, B. Nonlinear model predictive control(NMPC) of diesel oxidation catalyst (DOC) outlet temperature for active regeneration of diesel particulate filter (DPF) in diesel engine. *Energy* **2024**, *293*, 130658. [CrossRef]
19. Yu, X.; Wang, Y.; Wang, G.; Shen, Q.; Zeng, B.; He, S. Nonlinear Predictive Control of Diesel Engine DOC Outlet Temperature. *Processes* **2024**, *12*, 225. [CrossRef]
20. Huang, T.; Li, D.; Lu, J.; Luo, X.; He, W. Robust temperature control of a diesel oxidation catalyst using continuous terminal sliding mode with extended state observer. *Control Eng. Pract.* **2025**, *159*, 106316. [CrossRef]
21. Feng, Y.; Yu, X.; Han, F. On nonsingular terminal sliding-mode control of nonlinear systems. *Automatica* **2013**, *49*, 1715–1722. [CrossRef]
22. Shtessel, Y.; Edwards, C.; Fridman, L.; Levant, A. Sliding mode control and observation. In *Control Engineering*; Birkhäuser: New York, NY, USA, 2013. [CrossRef]
23. Yu, X.; Feng, Y.; Man, Z. Terminal Sliding Mode Control—An Overview. *IEEE Open J. Ind. Electron. Soc.* **2021**, *2*, 36–52. [CrossRef]
24. Wan, L.; Chen, G.; Sheng, M.; Zhang, Y.; Zhang, Z. Adaptive chattering-free terminal sliding-mode control for full-order nonlinear system with unknown disturbances and model uncertainties. *Int. J. Adv. Robot. Syst.* **2020**, *17*, 1–11. [CrossRef]
25. Feng, Y.; Han, X.; Wang, Y.; Yu, X. Second-order terminal sliding mode control of uncertain multivariable systems. *Int. J. Control* **2007**, *80*, 856–862. [CrossRef]
26. Liang, Y.; Zhang, D.; Li, G.; Wu, T. Adaptive Chattering-Free PID Sliding Mode Control for Tracking Problem of Uncertain Dynamical Systems. *Electronics* **2022**, *11*, 3499. [CrossRef]
27. Wang, M.-Y.; Yang, J.; Xiong, J.-J. Extended State Observer Based Nonsingular Terminal Sliding Mode Control for a Class of Dynamic Systems. In *Proceedings of the 2022 International Conference on Computer Engineering and Artificial Intelligence (ICCEAI)*; IEEE: Piscataway, NJ, USA, 2022; pp. 651–654. [CrossRef]
28. Wu, F.; Zhang, B.; Yao, D.; Yang, Y. Modeling and order reduction for the thermodynamics of a diesel oxidation catalyst with hydrocarbon dosing. *Catalysts* **2019**, *9*, 369–389. [CrossRef]
29. Goforth, F.; Zheng, Q.; Gao, Z. A novel practical control approach for rate independent hysteretic systems. *ISA Trans.* **2012**, *51*, 477–484. [CrossRef]
30. Feng, Y.; Yu, X.; Man, Z. Non-singular terminal sliding mode control of rigid manipulators. *Automatica* **2002**, *38*, 2159–2167. [CrossRef]
31. Huang, T.; Hu, G.; Guo, F.; Yang, M. A model-based research on exhaust temperature control for DPF active regeneration. *Automot. Eng.* **2019**, *41*, 133–139. [CrossRef]
32. Sampara, C.S.; Bissett, E.J.; Chmielewski, M. Global Kinetics for a Commercial Diesel Oxidation Catalyst with Two Exhaust Hydrocarbons. *Ind. Eng. Chem. Res.* **2008**, *47*, 311–322. [CrossRef]
33. Ning, J.; Yan, F. Composite control of DOC-out temperature for DPF regeneration. *IFAC-PapersOnLine* **2016**, *49*, 20–27. [CrossRef]
34. Synák, F.; Synák, J.; Skrúcaný, T.; Milojević, S. Modification of Engine Control Unit Data and Selected Vehicle Characteristics. *Appl. Eng. Lett.* **2019**, *4*, 120–127. [CrossRef]

Disclaimer/Publisher's Note: The statements, opinions and data contained in all publications are solely those of the individual author(s) and contributor(s) and not of MDPI and/or the editor(s). MDPI and/or the editor(s) disclaim responsibility for any injury to people or property resulting from any ideas, methods, instructions or products referred to in the content.